Crystal Structure of *Paracoccus denitrificans* Electron Transfer Flavoprotein: Structural and Electrostatic Analysis of a Conserved Flavin Binding Domain[†,‡]

David L. Roberts,[§] Denise Salazar,[||] John P. Fulmer,[§] Frank E. Frerman,[||] and Jung-Ja P. Kim*[,§]

Department of Biochemistry, Medical College of Wisconsin, Milwaukee, Wisconsin 53226, and Department of Pediatrics and the Cell and Developmental Biology Program, University of Colorado Health Sciences Center, Denver, Colorado, 80262

Received August 27, 1998; Revised Manuscript Received December 7, 1998

ABSTRACT: The crystal structure of electron transfer flavoprotein (ETF) from *Paracoccus denitrificans* was determined and refined to an *R*-factor of 19.3% at 2.6 Å resolution. The overall fold is identical to that of the human enzyme, with the exception of a single loop region. Like the human structure, the structure of the *P. denitrificans* ETF is comprised of three distinct domains, two contributed by the α-subunit and the third from the *β*-subunit. Close analysis of the structure reveals that the loop containing *β*I63 is in part responsible for conferring the high specificity of AMP binding by the ETF protein. Using the sequence and structures of the human and *P. denitrificans* enzymes as models, a detailed sequence alignment has been constructed for several members of the ETF family, including sequences derived for the putative FixA and FixB proteins. From this alignment, it is evident that in all members of the ETF family the residues located in the immediate vicinity of the FAD cofactor are identical, with the exception of the substitution of serine and leucine residues in the W3A1 ETF protein for the human residues αT266 and *β*Y16, respectively. Mapping of ionic differences between the human and *P. denitrificans* ETF onto the structure identifies a surface that is electrostatically very similar between the two proteins, thus supporting a previous docking model between human ETF and pig medium-chain acyl-CoA dehydrogenase (MCAD). Analysis of the ionic strength dependence of the electron transfer reaction between either human or *P. denitrificans* ETF and MCAD demonstrates that the human ETF functions optimally at low (∼10 mequiv) ionic strength, while *P. denitrificans* ETF is a better electron acceptor at higher (>75 mequiv) ionic strength. This suggests that the electrostatic surface potential of the two proteins is very different and is consistent with the difference in isoelectric points between the proteins. Analysis of the electrostatic potentials of the human and *P. denitrificans* ETFs reveals that the *P. denitrificans* ETF is more negatively charged. This excess negative charge may contribute to the difference in redox potentials between the two ETF flavoproteins and suggests an explanation for the opposing ionic strength dependencies for the reaction of MCAD with the two ETFs. Furthermore, by analysis of a model of the previously described human−*P. denitrificans* chimeric ETF protein, it is possible to identify one region of ETF that participates in docking with ETF-ubiquinone oxidoreductase, the physiological electron acceptor for ETF.

The heterodimeric electron transfer flavoproteins (ETF) function as intermediate electron carriers between primary dehydrogenases and terminal respiratory systems. They have been functionally classified by Weidenhaupt et al. (*1*) into "housekeeping" ETFs and those ETFs that are synthesized by prokaryotes under special nutritional conditions. The housekeeping ETFs function in the oxidation of fatty acids and some amino acids and include those isolated from mammals (*2*) and *Paracoccus denitrificans* (*3, 4*). The second group functions in the oxidation of secondary metabolites such as trimethylamine (*5*) carnitine (*6, 7*) and in nitrogen fixation (*8*). In the latter case, the ETF protein is proposed to link substrate oxidation to the reduction of a cbb_3-type terminal oxidase to provide energy for nitrogen fixation (*9*).

Overall sequence similarity within the ETF family ranges from about 25% among functionally unrelated ETF proteins to 60%−70% among functionally related heterodimers (*1*). The greatest amino acid sequence variation lies within the amino-terminal region of the α-(large) subunits, which forms domain I, a domain that does not participate in cofactor binding. Domain I was proposed to aid in the association of domains II and III, in a manner that facilitates FAD binding (*10*). On the other hand, the primary sequence of the carboxyl-terminal region of the α-subunits of the entire superfamily retains extremely high sequence identity. The three-dimensional structure of human ETF shows that the FAD prosthetic group is bound almost exclusively by the C-terminal domain of the α-subunit, though the dimethylbenzene ring of the flavin does make van der Waals contact with some residues within the *β*-subunit (*10*). Oxidation/reduction potentials for the oxidized/semiquinone form of the FAD cofactor vary among the ETF family, with the human (*11*) and pig (*12*) proteins residing around 0 mV, while the W3A1 protein has a potential of approximately

[†] This work was supported by NIH Grants GM29076 (J.-J.P.K.) and DK49726 (F.E.F.) and NRSA Grant DK09157 (D.L.R.).

[‡] The PDB accession code is 1EFP.

* To whom correspondence should be addressed.

[§] Medical College of Wisconsin.

[||] University of Colorado Health Sciences Center.

10.1021/bi9820917 CCC: $18.00
Published on Web 01/26/1999

+200 mV (*13*). Despite this wide range of redox potentials, the residues in the immediate vicinity of the FAD moiety are highly conserved throughout the family, with the exception of substitutions of αT266S and βY16L (human ETF numbering) by the W3A1 protein and αH286P by the *Megasphaera elsdenii* protein. Substitution in the human protein of βY16 with a leucine residue does change the fluorescence spectra observed for the purified protein but has little effect on the redox potential for the FAD (*14*). This suggests that, at least between the human and W3A1 ETF proteins, the residues in the immediate vicinity of the flavin do not play the exclusive role in modulating the difference in redox potentials observed. Adenosine 5′-monophosphate has been identified in the ETFs from *P. denitrificans* and human (*15*), pig (*16*), and the methylotrophic bacterium W3A1 (*17, 18*). This nucleotide, apparently involved in the folding of ETFs (*15, 16, 18*), is bound exclusively within the β-subunit, as determined by the three-dimensional structure of the human enzyme (*10*).

Mammalian and *P. denitrificans* ETFs can substitute for each other in several redox reactions, which is not surprising given the high amino acid sequence identity/similarity within the vicinity of the flavin that can be inferred from the human ETF structure. However, there are significant functional differences between the two proteins. *P. denitrificans* ETF will function as an electron acceptor for mammalian medium-chain and short-chain acyl-CoA dehydrogenases but will not oxidize a mammalian dimethylglycine dehydrogenase. Also, *P. denitrificans* ETF was previously reported as being incapable of transferring electrons to a mammalian ETF-ubiquinol oxidoreductase (ETF-QO), although mammalian ETF will reduce *P. denitrificans* ETF-QO (*3*). Previously, a chimeric human−*Paracoccus* ETF protein was constructed in which the first 84 residues of the human β-subunit were substituted by those of the *P. denitrificans* sequence (*19*). While this region still retains 64% sequence identity with the original human ETF protein, this chimeric ETF was found to be markedly diminished in the reaction between ETF and ETF-QO, suggesting that residues within the N-terminal portion of the β-subunit are necessary for interactions with ETF-QO (*19*). Furthermore, the redox behavior of *P. denitrificans* ETF is different from mammalian ETFs. The redox potentials of the bacterial ETF have not been directly determined; however, the formation constants of 1.6 for the human and 1.4−1.6 for the porcine ETF flavin semiquinones

$$ETF_{ox} + ETF_{2e^-} \rightleftharpoons 2ETF_{1e^-}$$

are approximately 2-fold greater than the corresponding value of 0.7 for the bacterial ETF semiquionone (*15*). This result indicates that the separation in the potentials of the two redox couples for the bacterial protein is less than the corresponding difference for the human and pig ETFs.

Recent studies of bacterial flavodoxins have provided insight regarding factors that modulate redox potentials in flavoproteins, including stacking of aromatic amino acid residues with the flavin ring, conformational changes and solvent accessibility, and charge dipoles (*20*−*22*). To assess the nature of the differences between the *P. denitrificans* and human ETF proteins, and to relate these differences with the overall structure, we have determined the three-dimensional structure of the *P. denitrificans* ETF. Close analysis of the AMP binding site indicates that the loop containing βI63 is in part responsible for binding AMP, while diminishing the binding of other nucleotides, such as IMP or GMP. Together with previously determined sequences for other members of the ETF superfamily of proteins, we have constructed a structure-based sequence alignment to identify conserved regions in the three-dimensional structure. Analysis of the structural alignment reveals regions where electrostatic differences occur between the proteins. From this analysis, we have identified several surface residues that may participate in the association of the human ETF with ETF-QO and support previous modeling studies for the docking of ETF and MCAD (*10*). In addition, from the differences in electrostatic potentials for the human and *P. denitrificans* ETF structures, we propose an explanation for the contrasting ionic strength dependencies of the reaction of human and *P. denitrificans* ETFs with porcine MCAD. Finally, this paper includes a study of the ionic strength dependence of the kinetic properties of the human, *P. denitrificans*, and chimeric ETF.

MATERIALS AND METHODS

Purification and Crystallization of P. denitrificans ETF. *P. denitrificans* ETF was purified and crystallized as previously described (*4, 23*). Briefly, cDNAs encoding ETF subunits were inserted into pBluescript SK^+, expressed in *Escherichia coli* DH5α, and the resulting ETF protein was purified by chromatography on DEAE Bio-Gel and hydroxylapatite. The A_{270nm}/A_{436nm} ratio of the purified protein used for crystallization studies was 5.8. For crystallization studies, the purified *P. denitrificans* ETF protein was dialyzed and concentrated against 10 mM Tris, pH 7.4. Crystals were formed by vapor diffusion using the hanging drop technique (*24*) by mixing equal volumes of the purified ETF protein (12 mg/mL) with the precipitating solution [18% (w/v) poly(ethylene glycol) (PEG) 8000, 25 mM KH_2PO_4, 100 μM FAD, and 5 mM $MgCl_2$, final pH of 5.8] and equilibrating against the precipitating solution at 19 °C.

X-ray Diffraction Data Collection. All data collection was performed using Cu Kα radiation from a Rigaku Rotaflex rotating anode generator (RU-200) operating at 50 kV and 100 mA with a graphite monochromator. The *P. denitrificans* ETF crystal was mounted in a thin-walled glass capillary tube, and diffraction data to 2.6 Å resolution were collected on a single crystal at 24 °C on an R-axis IIC image plate detector system. Still photographs indicated that the crystals belong to the orthorhombic space group $P2_12_12_1$, with unit cell parameters $a = 70.43$ Å, $b = 80.53$ Å, and $c = 183.97$ Å. Assuming two $\alpha\beta$ heterodimers per asymmetric unit, the calculated V_m value is 2.3 $Å^3$/Da (*25*). The oscillation method was used for data collection, using 1.1° oscillation per frame at a crystal to detector distance of 200 mm with $2\theta = 9°$. Data reduction and scaling were performed using the HKL package (*26*), and data set statistics are given in Table 1.

Structure Determination. The structure of *P. denitrificans* ETF was solved by the molecular replacement method (*27*) using the X-PLOR program package (*28*). *P. denitrificans* ETF shares approximately 54% amino acid sequence identity with human ETF; therefore, the refined coordinates of human ETF were used as the search model (PDB code 1EFV). None of the amino acids from the human ETF model were replaced

Table 1: Data Collection Statistics

parameters	wild type
resolution (A)	2.60
total no. of reflections[a]	118452
unique reflections	28666
R_{sym} (%)[b]	5.4
completeness (%)	87.8
space group	$P2_12_12_1$
unit cell dimensions (Å)	
a	70.43
b	80.53
c	183.97
final *R*-factor (%)	19.3
R_{free} (%)	28.6
no. of water molecules	101
deviations in rms geometry	
bond length (Å)	0.007
bond angles (deg)	1.4

[a] For all reflections with $I/\sigma > 0$. [b] $R_{sym} = \Sigma|I - \langle I\rangle|/\Sigma\langle I\rangle$, summed over all observations of all reflections.

with the corresponding residues from the *P. denitrificans* ETF prior to performing the search.

(1) Rotation Search. With a single heterodimeric human ETF molecule as the probe, a cross-rotation search was conducted using the Patterson search procedure as implemented in the X-PLOR package. Dimensions of the artificial cell searched were $a = b = c = 180$ Å, and the angular search interval was set to 1.5°. The 8430 reflections whose intensities were greater than 5σ in the resolution range 15−4 Å were used.

(2) Translation Search. The translation search was carried out using the search molecule with Eulerian angles that gave the highest peak in the rotation search (147.65, 27, 102.65) and employed a standard linear correlation coefficient between normalized, observed structure factors and normalized, calculated structure factors. Diffraction data with a resolution between 15 and 4 Å were used, and searches were performed in the range $x, y = 0-0.5$ and $z = 0-1.0$, with a sampling interval of 2 Å.

Structure Refinement. Refinement was carried out using iterative cycles of X-PLOR energy minimization followed by manual fitting and rebuilding on a Silicon Graphics workstation using TURBO−FRODO graphics software (*29*). In general, one round of X-PLOR refinement consisted of rigid body minimization, Powell positional refinement, a slow-cool simulated annealing beginning at 3000 K, and a second positional refinement. Later cycles also included refinement of the group and/or individual temperature factors. The two molecules in the asymmetric unit were refined using noncrystallographic symmetry (NCS) restraints until the *R*-factor was approximately 25%, at which point the NCS restraints were relaxed from a value of 300−150 kcal mol^{-1} Å^{-2}. When the *R*-factor reached 21%, the NCS restraints were further relaxed to 10 kcal mol^{-1} Å^{-2}.

After each cycle of X-PLOR refinement, both $2|F_o| - |F_c|$ and $|F_o| - |F_c|$ difference Fourier maps were calculated. When needed to clarify problematic regions, simulated annealing difference Fourier omit maps were calculated starting at 1000 K. These maps were then used to carry out manual fitting and rebuilding of the model. At later stages of refinement, water molecules were assigned when densities greater than 3σ were observed in the $|F_o| - |F_c|$ electron density map and were within at least 3.3 Å of a potential hydrogen-bonding partner.

Sequence Alignments. Amino acid sequences that are homologous to that of ETF were identified using the BLAST search algorithm using the sequence for human ETF as the search probe. Multiple alignments were then performed using the BESTFIT program of the GCG package (Wisconsin Package release 7.3, Genetics Computer Group, Madison, WI). The alignments were manually modified by attempting to place all gaps and insertions out of areas of secondary structure and into the more variable loop regions. The alignment between the human and *P. denitrificans* ETFs was based entirely on the three-dimensional structural overlap of the two proteins.

Electrostatic Potential Calculations. Molecular surfaces and electrostatic mapping were generated by the program Delphi within the Insight II package (Insight II Users Guide, 1995, Biosym/MSI, San Diego, CA) and viewed with the program GRASP (*30*). The electrostatic potential was calculated using a simple version of a Poisson−Boltzmann solver and mapped at the surface by means of a color ramp. Electrostatic potentials were calculated at the indicated ionic strengths, at a constant pH of 8.0. Dielectric constants used were 2 and 80 for the interior and exterior of the proteins, respectively.

Redox Potential Determinations. The redox potential of *P. denitrificans* ETF was determined at 10 °C by the xanthine/xanthine oxidase method as described (*31*). Reactions contained 10 mM potassium phosphate, pH 7.0, 10% glycerol, 250 μM xanthine, 50 nM xanthine oxidase, 2 μM benzyl viologen, 15−20 μM ETF, and pyocyanine equimolar with ETF. Pyocyanine ($E^{\circ\prime} = -34$ mV) was synthesized from phenazine methosulfate as described by McIlwain (*32*). The concentration of oxidized pyocyanine was determined by the absorbance at 690 nm ($\epsilon_{690nm} = 6.2 \times 10^3$ M^{-1}). The potentials of the flavin redox couples of *P. denitrificans* ETF are not widely separated (*15*), and after correction for the dye absorbance at 370 nm, it was not possible to detect stabilization of significant levels of semiquinone and the isosbestic point of the oxidized and semiquinone species at 482 nm was rapidly lost. Therefore, the data were calculated using $\Delta\epsilon_{ox-hq} = 11.2 \times 10^3$ M^{-1} at 436 nm and were treated as the overall potential for a two-electron transfer. Data were plotted according to Minnaert (*33*).

Enzyme Assays. The steady-state rate of reduction of human and *P. denitrificans* ETFs by pig MCAD was determined fluorometrically under anaerobic conditions as described (*34*). The reaction between the ETFs and pig ETF-QO was assayed by the catalyzed disproportionation ETF semiquinone reaction (*35*). The effect of ionic strength on both activities was determined by varying the NaCl concentration in the assay mix.

RESULTS AND DISCUSSION

Molecular Replacement Solution. Patterson correlation refinement of the 100 strongest peaks from the rotation search resulted in the emergence of only one strong peak, with a Patterson correlation of 0.085. From this, the search model with the Eulerian angles $\theta_1, \theta_2, \theta_3 = 147.65, 27, 102.65$ was chosen for the translation search. The translation search yielded a single peak at 30.36, 8.68, 151.23 Å along the

Table 2: Refinement Progress

rounds of X-PLOR refinement	*R*-factor (%)	R_{free} (%)	resolution (Å)	no. of reflections ($I/\sigma > 3$)	noncrystallographic symmetry wt (kcal mol^{-1} A^{-2})
start[a]	43.4	nd	15.0−3.0	19 167	na
1[b]	27.5	38.5	15.0−2.6	26 506	na
2[c]	29.3	37.1	15.0−2.6	23 824	300
3[d]	25.7	34.1	15.0−2.6	26 506	300
4−5	23.1	32.6	10.0−2.6	26 105	300
6[e]	19.3	28.6	12.0−2.6	25 185	100 main chain/5 side chain

[a] The starting molecule begins after location of the noncrystallographic symmetry axis and consists only of rigid-body refinement. This model also consists entirely of the human ETF sequence. [b] At this stage, all of the residues for the *P. denitrificans* ETF have been inserted.[c] Begin using noncrystallographic symmetry restraints. [d] Beginning with round 3, grouped *B*-factors were refined at the end of each cycle. [e] 101 water molecules were added beginning at round 6. At this time, NCS restraints were relaxed from 300 to 100 for main chain and from 300 to 5 for side chains.

crystallographic axes *a*, *b*, and *c*, with a peak height/σ of 19.6. The initial *R*-factor was 49.1%, with only one of the two heterodimers within the asymmetric unit.

Location of the Noncrystallographic Symmetry Axis. Neither a self-rotation function nor cross-rotation search revealed the location of the noncrystallographic symmetry axis, suggesting that the noncrystallographic 2-fold axis is parallel to a crystallographic axis. In an attempt to locate the position of the second molecule of ETF within the asymmetric unit, a self-Patterson map was calculated, revealing a large peak at 0, 0.48, 0.22, with a magnitude corresponding to 8% of the origin peak, thus locating the Patterson vector between the two noncrystallographically related molecules. This Patterson vector was applied to the solution from the translation search, and the four crystallographic symmetry operations were applied to the resultant molecule. From this, one molecule was identified that was related to the original molecule by a 2-fold rotation axis located at x, $z = 0.50$, 0.11, and approximately parallel to the *y*-axis.

Refinement of the Structure of P. denitrificans ETF. Once the crystallographic 2-fold axis was established, the molecular replacement phases were improved, reducing the *R*-factor from 49.1% to 43.4%, by simply employing only one round of energy minimization consisting of rigid-body refinement. At this stage, manual rebuilding of the model was performed. The correct residues for *P. denitrificans* ETF were inserted in the structure when density was observed in the difference Fourier maps. When no clear density was observed for the side chains, an alanine was modeled into the structure. After two cycles of energy minimization, consisting of rigid-body, Powell positional, and simulated annealing refinement, and manual rebuilding of the model, the entire sequence for the *P. denitrificans* ETF was correctly incorporated into the model. The *R*-factor at this point was 27.5%, with a free *R*-factor of 38.5% for the 26 506 reflections between 15.0 and 2.6 Å resolution with $I/\sigma >$ 3.0. Table 2 indicates the refinement progress with the structure determination of *P. denitrificans* ETF. After a total of six repetitive cycles of energy minimization refinement followed by manual adjustment of the model, the final *R*-factor after the addition of 101 water molecules was 19.3%, with a free *R*-factor of 28.6% for the 25 185 reflections between 12.0 and 2.6 Å resolution with $I/\sigma > 1.0$. The final model of the *P. denitrificans* ETF protein, complete with one molecule of FAD and AMP and not including the 101 water molecules, contains 8192 non-hydrogen atoms. Beginning in the α-subunit with αA2, the density is continuous throughout the entire polypeptide chain, to αL308. The *β*-subunit, beginning with *β*M1, shows continuous density through residue *β*L246, with no observed density for the carboxyl-terminal six residues (KEAGVI).

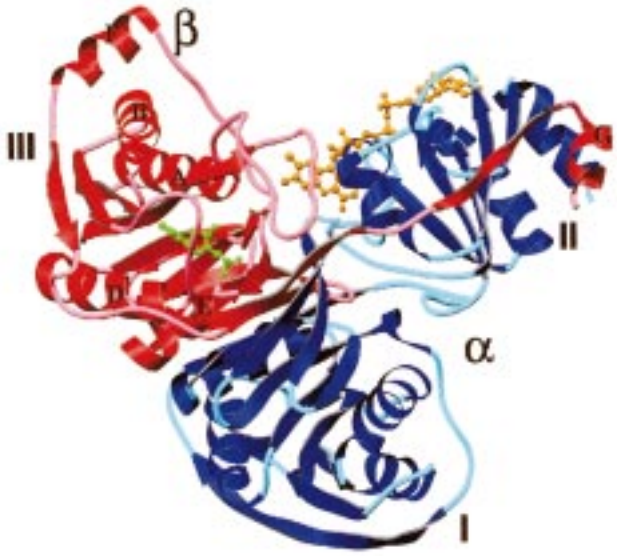

FIGURE 1: Ribbon diagram of the *P. denitrificans* ETF structure. The structure is comprised of three distinct domains. Domains I and II are contributed by the (α-subunit) (cyan/blue ribbon), while domain III is made up exclusively by the (beta) (red/rose). FAD (orange ball-and-stick model) binds in a cleft formed by domains II and III, while AMP (green ball-and-stick model) binds exclusively within domain III. For clarity, only helices mentioned in the text are labeled. All ribbon models were generated using the program RIBBONS (*36*).

The statistics for the *P. denitrificans* ETF protein are reported in Table 1. The average *B*-factor value for the main-chain polypeptide backbone is 26.9 Å^2, and the average side-chain *B*-factor is 29.1 Å^2. Ramachandran plot analysis indicates that, for main-chain dihedral angles, 87% of the residues reside in the most favored regions, while none are observed in disallowed or generously allowed regions. In the human structure, αK226 falls in the disallowed region of the Ramachandran plot, due to crystal packing contacts (*10*). The corresponding residue in *P. denitrificans* ETF is a glycine residue (αG204) and therefore does not have any dihedral restraints. The root-mean-square (rms) deviations from ideal values of the bond lengths and bond angles of the ETF model are 0.007 Å and 1.4°, respectively.

Description of the P. denitrificans ETF Structure. As shown in Figure 1, the overall fold of the *P. denitrificans* ETF protein is identical to that of the human ETF protein. The rms deviation between the main-chain atoms of *P. denitrificans* ETF and human ETF is 0.56 Å, excluding variable loop regions (410 of the 543 total residues). As with the human ETF protein, the structure of the *P. denitrificans* ETF protein consists of three distinct domains. Domains I and II comprise the N- and C-terminal portions of the α-subunit, respectively, while domain III consists entirely of the *β*-subunit (*10*). FAD resides in a cleft between the

C-terminal half of the α-subunit (domain II) and the β-subunit (domain III), while AMP lies entirely within the β-subunit.

While the overall topology is essentially identical between the human and *P. denitrificans* ETF structures, there are two structural differences that are worth noting. The first involves comparing the overall fold of the two proteins. The only difference in the fold of the *P. denitrificans* ETF protein compared to the human form is a loop located within the β-subunit, between residues β90 and β96. In the *P. denitrificans* ETF structure this loop is in the form of a random coil, while in the human structure this region folds into an α-helix. The role of this region is not clear, since this is a highly variable region in all the sequences of the ETF family of proteins (see below).

The second difference between the two proteins involves the relative location of domains I, II, and III with respect to one another. Overlap of the human and *P. denitrificans* structures reveals that domains II and III (the domains responsible for binding FAD) superimpose well, with an rmsd of approximately 0.46 Å for Cα atoms. However, domain I is twisted approximately 4° when comparing the *P. denitrificans* structure to the human ETF, resulting in an rmsd between domain I of the two proteins of 1.1 Å. When looking closely at these differences, however, it is interesting to note that, in domain I, residues at the heterodimer interface are relatively fixed between the two proteins, while residues that are located at the "bottom" of the molecule (as shown in Figure 1), which do not participate in any domain interactions, are the ones that are twisted most between the two structures. The rmsd between the two structures is as large as 2.7 Å for Cα atoms of the residues located within the loop between helix F and strand 7. The significance of this point is not clear. It is not likely to have anything to do with donor and acceptor specificity, since the only region known to alter reactions with primary dehydrogenases and ETF-QO is the amino-terminal region of the β-subunit (domain III), which has been determined by study of the chimeric ETF (*19*). It is possible that the ETF protein is flexible in solution and that the domains are capable of shifting with respect to one another. This flexibility may function in electron transfer reactions, enabling the domains to shift and "conform" to the topology of the specific electron transfer partner.

Residues Involved in Binding AMP. Consistent with the structure of human ETF, the structure of *P. denitrificans* ETF also contains one molecule of noncovalently bound AMP deeply buried within the β-subunit. A single tightly bound molecule of AMP has also been detected in the ETFs from bacterium W3A1 (17), pig (*16*), and human (*10*, *15*). Figure 2A shows a stereoview of the AMP binding site. The residues from *P. denitrificans* ETF superimpose well with those of the human enzyme, with an rmsd of approximately 0.15 Å among similar atoms involved in binding AMP. The interactions between ETF and the AMP involve primarily main-chain atoms of the polypeptide, with few interactions occurring between side-chain atoms and the AMP moiety. Attempts to reconstitute the AMP-free ETF protein with other nucleotides (IMP, GMP, and UMP) and the nucleoside, adenosine, have failed. Close analysis of the structure reveals a few residues that may be imparting this high degree of nucleotide specificity. The phosphate moiety of AMP is located within a helical dipole at the N-terminal end of helix E. It forms several hydrogen bonds with the protein, including residues A123, N126, N129, A130, and T131, all from the β-subunit. Failure of the nucleoside adenosine to bind to the apo-ETF protein is presumably due to the loss of these interactions with the phosphate moiety. For both IMP and GMP, N1 of the purine ring is protonated, while N1 in AMP is not. The N1 of AMP is a hydrogen bond acceptor for the backbone amide of βI63. In the case of IMP and GMP, the presence of the N1 hydrogen would lead to an unfavorable interaction with the amide hydrogen of βI63, thus destabilizing nucleotide binding. Furthermore, the C6 amino group of AMP forms a hydrogen bond with the main-chain carbonyl group of βI63. Replacement of the C6 amino group with a carbonyl group (as in IMP and GMP) would abolish this important hydrogen bond and thus lower the binding affinity for these nucleotides. 8-Azido-AMP will also support reconstitution of human and *P. denitrificans* ETF, but only 30% as well as AMP (Dwyer and Frerman, unpublished). It appears that one binding determinant may be the six-membered ring of the purine. While it is not clear what the specific role of AMP is in ETF, it is thought that this AMP binding site may be a remnant of an NAD(H) binding site in ancestral ETF proteins, since the ETF from *M. elsdenii* does not bind AMP and utilizes NADH as the reductant (*37*, *38*). NADH does not bind to either human or *P. denitrificans* ETF proteins, but superposition of the AMP moiety of NADH within the AMP binding site places the nicotinamide ring within 5 Å of the flavin ring, a distance close enough for direct electron transfer. However, if this is indeed a vestigial NADH binding site, the structure of the *M. elsdenii* ETF protein would need to have some differences in this region in order to properly accommodate the pyrimidine nucleotide cofactor. It is also possible that, at least in the *M. elsdenii* ETF, a second molecule of FAD binds within this site. Further analysis will have to await the structural elucidation, which is presently underway (*39*).

Residues Involved in Binding FAD. Figure 2B shows a stereoview of residues involved in binding the isoalloxazine portion of the FAD cofactor. The residues located within the immediate vicinity of the flavin ring are identical for all members of the ETF family, with the exception of serine and leucine for αT266 and βY16 (human numbering; the corresponding residues in *P. denitrificans*, αT244 and βY13), respectively, in the W3A1 protein (*5*), and proline for αH286 in *M. elsdenii* ETF *(38*). By using flavin analogues in which increasingly bulky substituents are placed on the 8 position of the FAD ring, Gorelick and Thorpe (*40*) demonstrated that the 8 position of the isoalloxazine ring is exposed to solvent. The results demonstrated that substituents as large as a CoA moiety at the C8 position of the FAD are still capable of accepting electrons from MCAD, albeit at a rate considerably slower than the natural flavin. The slower rate could be due to either affecting the electron path between ETF and its electron partners or simply altering the binding specificity of MCAD for ETF. To accommodate these large substituents, Tyr16 of the β-subunit would have to shift, since it is forming hydrophobic interactions with the C8 methyl group of the FAD cofactor. Mutagenesis studies in which βY16 is replaced with a Leu residue indicate that while the flavin fluorescence spectrum is dramatically altered, the steady-state rate of ETF reduction is not affected (*14*). So,

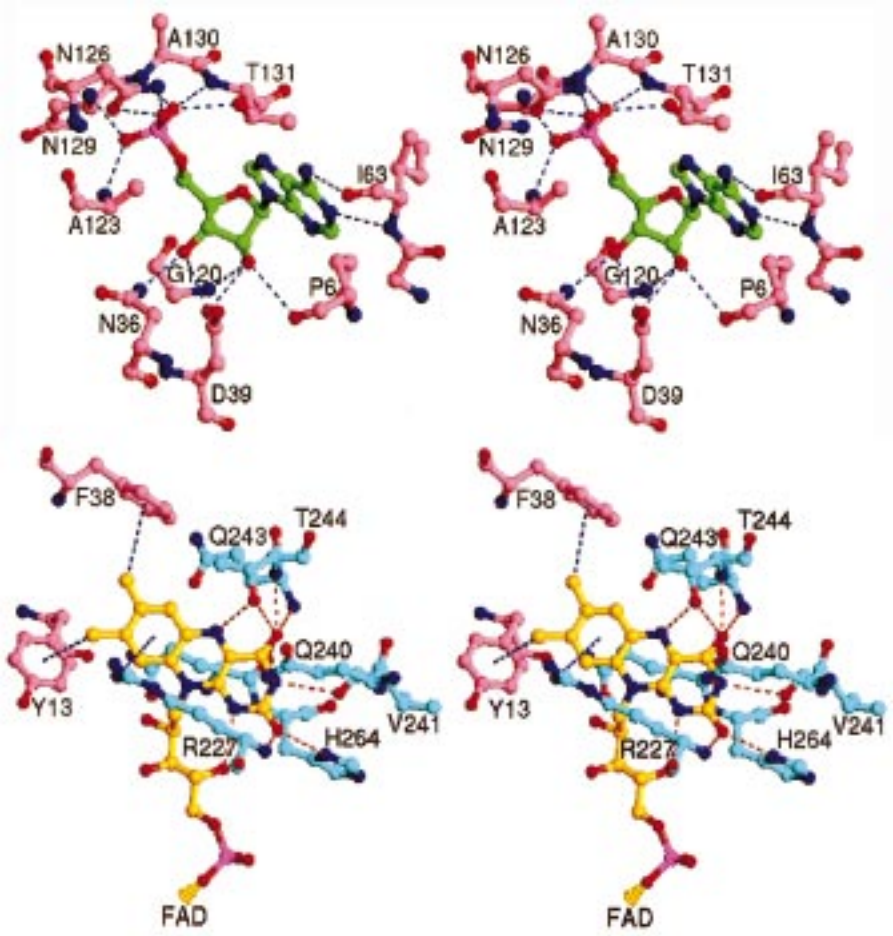

FIGURE 2: (A, top) Stereo diagram of the complex network of hydrogen bonds formed between AMP and ETF. Residues within the AMP binding site are shown (rose ball-and-stick model), along with AMP (green ball-and-stick model). Potential hydrogen bonds are indicated by blue dashed lines. Atoms are colored as follows: red, oxygen; blue, nitrogen; rose, protein carbon; green, AMP carbon; and lavender, phosphate. The numbering corresponds to that of the *P. denitrificans* ETF. (B, bottom) Stereo diagram of the complex network of hydrogen bonds formed between FAD and ETF. Residues within the FAD binding site are shown (rose and cyan ball-and-stick models), along with FAD (gold ball-and-stick model). Potential hydrogen bonds are indicated by red dashed lines, while stacking interactions (hydrophobic) are indicated by blue dotted lines. Atoms are colored as follows: red, oxygen; blue, nitrogen; cyan, carbon from domain II of ETF; rose, carbon from domain III of ETF, gold, FAD carbon; and lavender, phosphate.

while βY16 does interact with the flavin cofactor, it does not appear to participate in electron transfer reactions between ETF and its redox partners. Overlap of the human and *P. denitrificans* ETF structures reveals that not only the identity but also the positions of residues in the immediate vicinity of the FAD ring are highly conserved, with an rmsd of approximately 0.12 Å between all atoms in the vicinity of FAD binding.

A characteristic of the FAD binding site involves the hydrogen bond between the ribityl 4′-hydroxyl group and N1 of the flavin ring (2.9 Å). Analysis of all the protein structures containing either FAD or FMN cofactors reveals that only three structures have a similar hydrogen bond. The LuxF protein (*41*; PDB accession code 1NFP) binds to two FMN cofactors. One FMN has a 4′-hydroxyl group situated 2.9 Å from N1 of the flavin ring. Nitrate reductase (*42*; PDB code 1CNE) and pyruvate oxidase (*43*; PDB code 1POW) both contain FAD cofactors, and likewise both exhibit hydrogen bonding between the 4′-hydroxyl of the ribityl side chain and N1 of the flavin ring. Preliminary studies with ETF reconstituted with 4′-deoxy-FAD show that the reductive half-reaction with MCAD is reduced by 75%. On the other hand, the reaction with ETF-QO is undetectable in either direction, i.e., in the direction of ETF oxidation or reduction (Frerman, unpublished). This suggests that the 4′-hydroxyl group functions to stabilize the semiquinone/hydroquinone couple of the FAD. Furthermore, the results also indicate that the 4′-hydroxyl group is likely to be involved in the electron transfer between the ETF flavin and the ETF-QO flavin. ^{13}C and ^{15}N NMR spectroscopy of the flavin in human ETF indicates that the flavin N1 is hydrogen bonded in the oxidized state, consistent with the X-ray structure, and ionized in the two-electron reduced state, as observed in all other reduced flavoproteins investigated by ^{15}N NMR (*44*). These data also suggest that the hydrogen bond between 4′-OH and N1 in FAD is stronger in the reduced states in which negative charge is localized in the N1−C2O region of the flavin (*45*).

Another distinguishing characteristic of the ETF flavin binding domain is that there are no aromatic residues that stack parallel to the ring, which is often characteristic of flavin binding proteins. Instead, ETF contains an Arg residue (αR249, human numbering) in which the guanidinium portion of the Arg side chain is 3.7 Å away from and perpendicular to the xylene portion of the isoalloxazine ring. This positively charged Arg residue is conserved throughout

the entire ETF family of proteins (see below) and may function in stabilizing the anionic reduced species of ETF, in a manner that could not be accomplished by an aromatic residue. The only other flavoprotein with a similar Arg side chain is that of *p*-hydroxybenzoate hydroxylase (*46*; PDB code 1DOE), in which the flavin ring adopts two conformations. In the "in" form of the protein, the isoalloxazine ring is buried and undergoes hydroxylation by an aromatic substrate that is stacked with the flavin ring. In the absence of substrate, the flavin adopts the "out" form, in which R44 replaces the substrate in stacking with the flavin in a manner similar to R249 of ETF. From modeling of the docking between pig MCAD and human ETF, Roberts et al. have proposed that αR249 participates in the electron transfer pathway between the two proteins (*10*). This pathway would be consistent with electron transfer in the region of C8 proposed by Gorelich and Thorpe (*40*).

As seen in the structure of human ETF, the ADP moiety of the FAD is exposed and is located on the surface of domain II. The residues contacting this portion of the FAD cofactor are also conserved between the two ETFs, with one exception of a glycine (αG204 in *P. denitrificans*) replacing the corresponding residue αK226 of human ETF (*10*). With the exception of a hydrogen bond between ϵNH_2 of the lysine residue and the N7 atom of the adenine ring, all other interactions between the polypeptide and the ADP portion of the FAD are conserved in the two ETF structures.

Structural Alignment of Members of the ETF Family. Sequences of several ETFs have been reported, and three have been expressed as active proteins (*5*). Furthermore, bacterial ETFs referred to as *fix*A and *fixB* gene products have been identified on the basis of their sequence similarity to the ETF proteins. While the *fixA* and *fixB* gene products have not yet been purified, they are believed to be flavoenzymes, primarily due to the high sequence similarities within the flavin binding domain of ETF (*1*). The Fix proteins function in assimilating nitrogen, most likely as part of an electron transport chain that provides energy for nitrogen fixation, rather than in the reduction of the nitrogenase enzyme (*1*). The ETF and Fix proteins form a closely related family with no apparent homology to other known protein sequences. With the two ETF structures in hand, a structure-based sequence alignment was constructed (Figure 3). The secondary structure assignment corresponds to that previously published for the human ETF protein (*10*). The consensus sequence corresponds to residues that are identical in at least four of the sequences within the alignment. As previously discussed (*5*, *10*), residues in the C-terminal portion of the α-subunit are highly conserved. This region corresponds to domain II, which is the domain primarily responsible for binding FAD. In all of the sequences displayed in the alignment, the residues directly located around the FAD are identical, except for the conservative substitution of serine for threonine at position 266 in the W3A1 protein. These alignments also show that the AMP binding domain is also highly conserved. AMP binds ETF exclusively within the β-subunit, with residues in the binding site being contributed by those within strand 1, at the C-terminal end of strand 2, and from strands 4, 4a, and 4b (see Figure 3B). The phosphate moiety of the AMP is located at the center of a helical dipole formed by helix E. Last, the core residues belonging to the three domains that form the ETF protein also show high levels of sequence conservation, while the strands that "tie up" the domains and lie in hinge regions show little to no conservation, particularly between domains I and II in the α-subunit (Figure 3A, from helix F through the beginning of strand 8). On the basis of these alignments, it is probable that the overall topologies and structures of the ETF proteins are quite similar, although certain variable residues may confer specificity for electron donors and acceptors and modulate the redox potentials.

Mapping of Electrostatic Differences on the ETF Structure. Previous studies have shown that electrostatic interactions are the primary recognition force between ETF and its electron donors and acceptors (*34*, *35*). Furthermore, both the human and *P. denitrificans* ETFs have been shown to cross-react with several of the primary dehydrogenases, including porcine MCAD. Therefore, it is assumed that these two ETF proteins share an electrostatically similar "docking" surface for these common substrates. Figure 4 shows a ribbon diagram of the *P. denitrificans* ETF protein, with shading based on residues that are electrostatically altered between the human and *Paracoccus* ETFs. From this figure, it is clear that the most conserved domain is domain II, while domains I and III are the most divergent. Furthermore, the "top" surface of the ETF protein, which is in the vicinity of the FAD, is the most electrostatically conserved and therefore the most likely surface for common redox partners to interact. It was this surface that was previously proposed to be the docking site for MCAD on the human ETF (*10*) and is still the most likely surface for MCAD to dock with the ETF protein.

Surface Potential of the ETF Proteins. Because there are over 60 residues that change charge between the human and *P. denitrificans* ETF structures, and also since the p*I*'s are quite different between the two proteins (4.5 for *P. denitrificans* and 7.2 for the human), we calculated the electrostatic surface potential of the two proteins. Figure 5 shows the surface potentials and dipole direction as looking from the top of the ETF molecule, which is the proposed docking site for MCAD. The potentials were calculated at two different ionic strengths (10 and 145 mequiv) for three different ETF proteins (human, *P. denitrificans*, and a model of the chimeric ETF). The surface potential of the human ETF protein, which is displayed as an almost even mixture of positive and negative zones, is consistent with the near neutral p*I* of the human ETF (*19*). On the other hand, the surface potential calculation of the bacterial protein shows a very negatively charged protein, consistent with the p*I* of approximately 4.5. Furthermore, the electric dipole of the entire molecule is different (1100 D for human, 1100 D for the chimera, and 600 D for the *P. denitrificans* ETF), which may play some role in interaction between ETF and its redox partners, including MCAD. From these figures, it is clear that at 10 mequiv ionic strength the human and *P. denitrificans* surfaces are dramatically different, with the human ETF having more positive (blue) charges while the *P. denitrificans* ETF is predominantly negative (red) in charge. As the ionic strength is increased to 145 mequiv, the surfaces become electrostatically neutralized.

The three-dimensional structure of ETF-QO is not known; however, it is possible to locate at least one region that would participate in docking with ETF-QO. Like the reaction between ETF and MCAD, interactions between ETF and

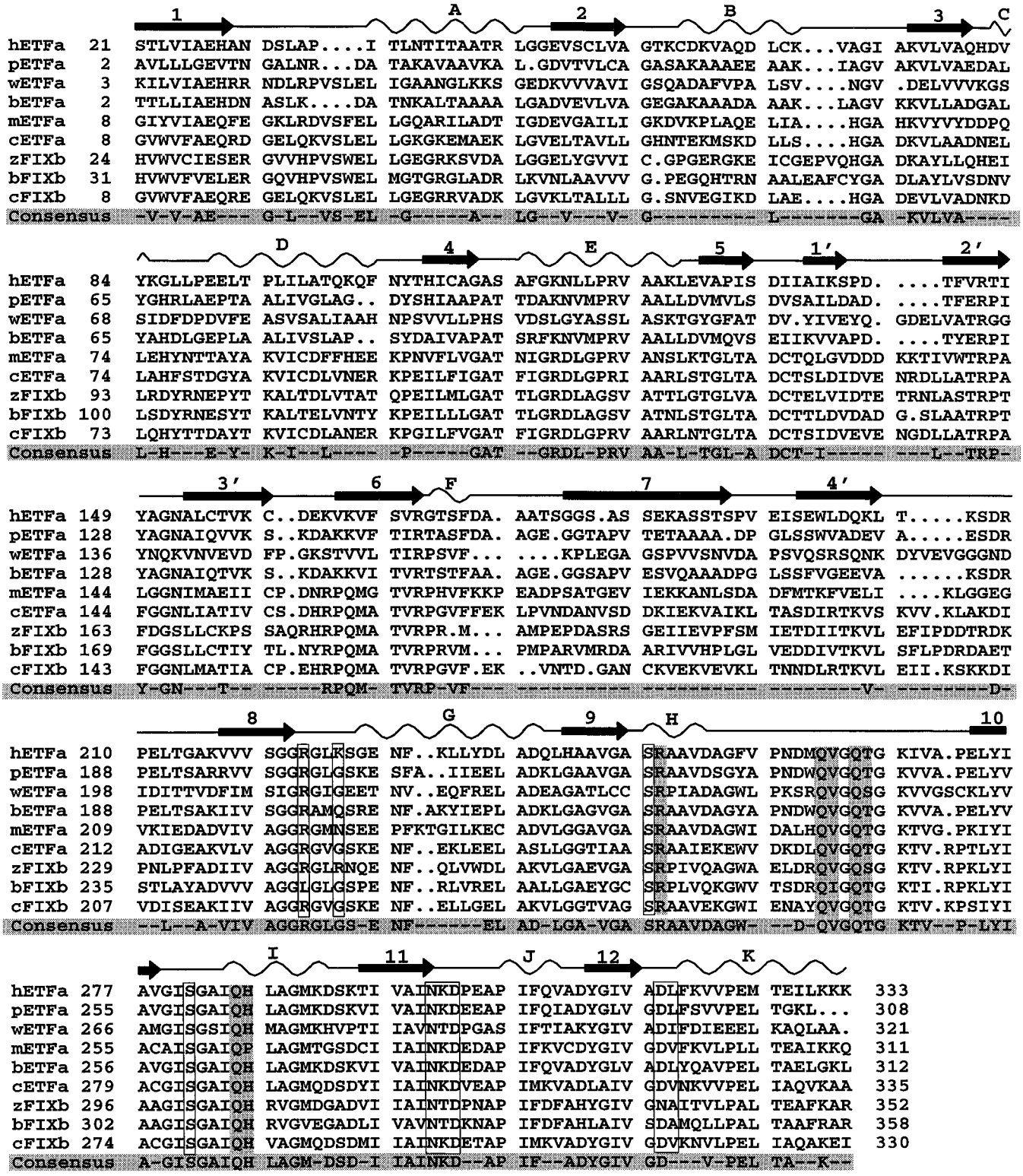
1 A 2 B 3 C
hETFa 21 STLVIAEHAN DSLAP....I TLNTITAATR LGGEVSCLVA GTKCDKVAQD LCK...VAGI AKVLVAQHDV
pETFa 2 AVLLLGEVTN GALNR...DA TAKAVAAVKA L.GDVTVLCA GASAKAAAEE AAK...IAGV AKVLVAEDAL
wETFa 3 KILVIAEHRR NDLRPVSLEL IGAANGLKKS GEDKVVVAVI GSQADAFVPA LSV....NGV .DELVVVKGS
bETFa 2 TTLLIAEHDN ASLK....DA TNKALTAAAA LGADVEVLVA GEGAKAAADA AAK...LAGV KKVLLADGAL
mETFa 8 GIYVIAEQFE GKLRDVSFEL LGQARILADT IGDEVGAILI GKDVKPLAQE LIA....HGA HKVYVYDDPQ
cETFa 8 GVWVFAEQRD GELQKVSLEL LGKGKEMAEK LGVELTAVLL GHNTEKMSKD LLS....HGA DKVLAADNEL
zFIXb 24 HVWVCIESER GVVHPVSWEL LGEGRKSVDA LGGELYGVVI C.GPGERGKE ICGEPVQHGA DKAYLLQHEI
bFIXb 31 HVWVFVELER GQVHPVSWEL MGTGRGLADR LKVNLAAVVV G.PEGQHTRN AALEAFCYGA DLAYLVSDNV
cFIXb 8 GVWVFAEQRE GELQKVSLEL LGEGRRVADK LGVKLTALLL G.SNVEGIKD LAE....HGA DEVLVADNKD
Consensus -V-V-AE--- G-L--VS-EL -G-----A-- LG--V---V- G--------- L------GA -KVLVA----
D 4 E 5 1′ 2′
hETFa 84 YKGLLPEELT PLILATQKQF NYTHICAGAS AFGKNLLPRV AAKLEVAPIS DIIAIKSPD. ....TFVRTI
pETFa 65 YGHRLAEPTA ALIVGLAG.. DYSHIAAPAT TDAKNVMPRV AALLDVMVLS DVSAILDAD. ....TFERPI
wETFa 68 SIDFDPDVFE ASVSALIAAH NPSVVLLPHS VDSLGYASSL ASKTGYGFAT DV.YIVEYQ. GDELVATRGG
bETFa 65 YAHDLGEPLA ALIVSLAP.. SYDAIVAPAT SRFKNVMPRV AALLDVMQVS EIIKVVAPD. ....TYERPI
mETFa 74 LEHYNTTAYA KVICDFFHEE KPNVFLVGAT NIGRDLGPRV ANSLKTGLTA DCTQLGVDDD KKTIVWTRPA
cETFa 74 LAHFSTDGYA KVICDLVNER KPEILFIGAT FIGRDLGPRI AARLSTGLTA DCTSLDIDVE NRDLLATRPA
zFIXb 93 LRDYRNEPYT KALTDLVTAT QPEILMLGAT TLGRDLAGSV ATTLGTGLVA DCTELVIDTE TRNLASTRPT
bFIXb 100 LSDYRNESYT KALTELVNTY KPEILLLGAT TLGRDLAGSV ATNLSTGLTA DCTTLDVDAD G.SLAATRPT
cFIXb 73 LQHYTTDAYT KVICDLANER KPGILFVGAT FIGRDLGPRV AARLNTGLTA DCTSIDVEVE NGDLLATRPA
Consensus L-H---E-Y- K-I--L---- -P-----GAT --GRDL-PRV AA-L-TGL-A DCT-I----- ---L--TRP-
3′ 6 F 7 4′
hETFa 149 YAGNALCTVK C..DEKVKVF SVRGTSFDA. AATSGGS.AS SEKASSTSPV EISEWLDQKL T.....KSDR
pETFa 128 YAGNAIQVVK S..KDAKKVF TIRTASFDA. AGE.GGTAPV TETAAAA.DP GLSSWVADEV A.....ESDR
wETFa 136 YNQKVNVEVD FP.GKSTVVL TIRPSVF... ....KPLEGA GSPVVSNVDA PSVQSRSQNK DYVEVGGGND
bETFa 128 YAGNAIQTVK S..KDAKKVI TVRTSTFAA. AGE.GGSAPV ESVQAAADPG LSSFVGEEVA ......KSDR
mETFa 144 LGGNIMAEII CP.DNRPQMG TVRPHVFKKP EADPSATGEV IEKKANLSDA DFMTKFVELI ....KLGGEG
cETFa 144 FGGNLIATIV CS.DHRPQMA TVRPGVFFEK LPVNDANVSD DKIEKVAIKL TASDIRTKVS KVV.KLAKDI
zFIXb 163 FDGSLLCKPS SAQRHRPQMA TVRPR.M... AMPEPDASRS GEIIEVPFSM IETDIITKVL EFIPDDTRDK
bFIXb 169 FGGSLLCTIY TL.NYRPQMA TVRPRVM... PMPARVMRDA ARIVVHPLGL VEDDIVTKVL SFLPDRDAET
cFIXb 143 FGGNLMATIA CP.EHRPQMA TVRPGVF.EK ..VNTD.GAN CKVEKVEVKL TNNDLRTKVL EII.KSKKDI
Consensus Y-GN---T-- -----RPQM- TVRP-VF--- ---------- ---------- ---------V- ---------D-
8 G 9 H 10
hETFa 210 PELTGAKVVV SGGRGLKSGE NF..KLLYDL ADQLHAAVGA SRAAVDAGFV PNDMQVGQTG KIVA.PELYI
pETFa 188 PELTSARRVV SGGRGLGSKE SFA..IIEEL ADKLGAAVGA SRAAVDSGYA PNDWQVGQTG KVVA.PELYV
wETFa 198 IDITTVDFIM SIGRGIGEET NV..EQFREL ADEAGATLCC SRPIADAGWL PKSRQVGQSG KVVGSCKLYV
bETFa 188 PELTSAKIIV SGGRAMQSRE NF.AKYIEPL ADKLGAGVGA SRAAVDAGYA PNDWQVGQTG KVVA.PELYV
mETFa 209 VKIEDADVIV AGGRGMNSEE PFKTGILKEC ADVLGGAVGA SRAAVDAGWI DALHQVGQTG KTVG.PKIYI
cETFa 212 ADIGEAKVLV AGGRGVGSKE NF..EKLEEL ASLLGGTIAA SRAAIEKEWV DKDLQVGQTG KTV.RPTLYI
zFIXb 229 PNLPFADIIV AGGRGLRNQE NF..QLVWDL AKVLGAEVGA SRPIVQAGWA ELDRQVGQSG KTV.RPKLYI
bFIXb 235 STLAYADVVV AGGLGLGSPE NF..RLVREL AALLGAEYGC SRPLVQKGWV TSDRQIGQTG KTI.RPKLYI
cFIXb 207 VDISEAKIIV AGGRGVGSKE NF..ELLGEL AKVLGGTVAG SRAAVEKGWI ENAYQVGQTG KTV.KPSIYI
Consensus --L--A-VIV AGGRGLGS-E NF------EL AD-LGA-VGA SRAAVDAGW- --D-QVGQTG KTV--P-LYI
I 11 J 12 K
hETFa 277 AVGISGAIQH LAGMKDSKTI VAINKDPEAP IFQVADYGIV ADLFKVVPEM TEILKKK 333
pETFa 255 AVGISGAIQH LAGMKDSKVI VAINKDEEAP IFQIADYGLV GDLFSVVPEL TGKL... 308
wETFa 266 AMGISGSIQH MAGMKHVPTI IAVNTDPGAS IFTIAKYGIV ADIFDIEEEL KAQLAA. 321
mETFa 255 ACAISGAIQP LAGMTGSDCI IAINKDEDAP IFKVCDYGIV GDVFKVLPLL TEAIKKQ 311
bETFa 256 AVGISGAIQH LAGMKDSKVI VAINKDEDAP IFQVADYGLV ADLYQAVPEL TAELGKL 312
cETFa 279 ACGISGAIQH LAGMQDSDYI IAINKDVEAP IMKVADLAIV GDVNKVVPEL IAQVKAA 335
zFIXb 296 AAGISGAIQH RVGMDGADVI IAINTDPNAP IFDFAHYGIV GNAITVLPAL TEAFKAR 352
bFIXb 302 AAGISGAIQH RVGVEGADLI VAVNTDKNAP IFDFAHLAIV SDAMQLLPAL TAAFRAR 358
cFIXb 274 ACGISGAIQH VAGMQDSDMI IAINKDETAP IMKVADYGIV GDVKNVLPEL IAQAKEI 330
Consensus A-GISGAIQH LAGM-DSD-I IAINKD--AP IF--ADYGIV GD---V-PEL TA--K--

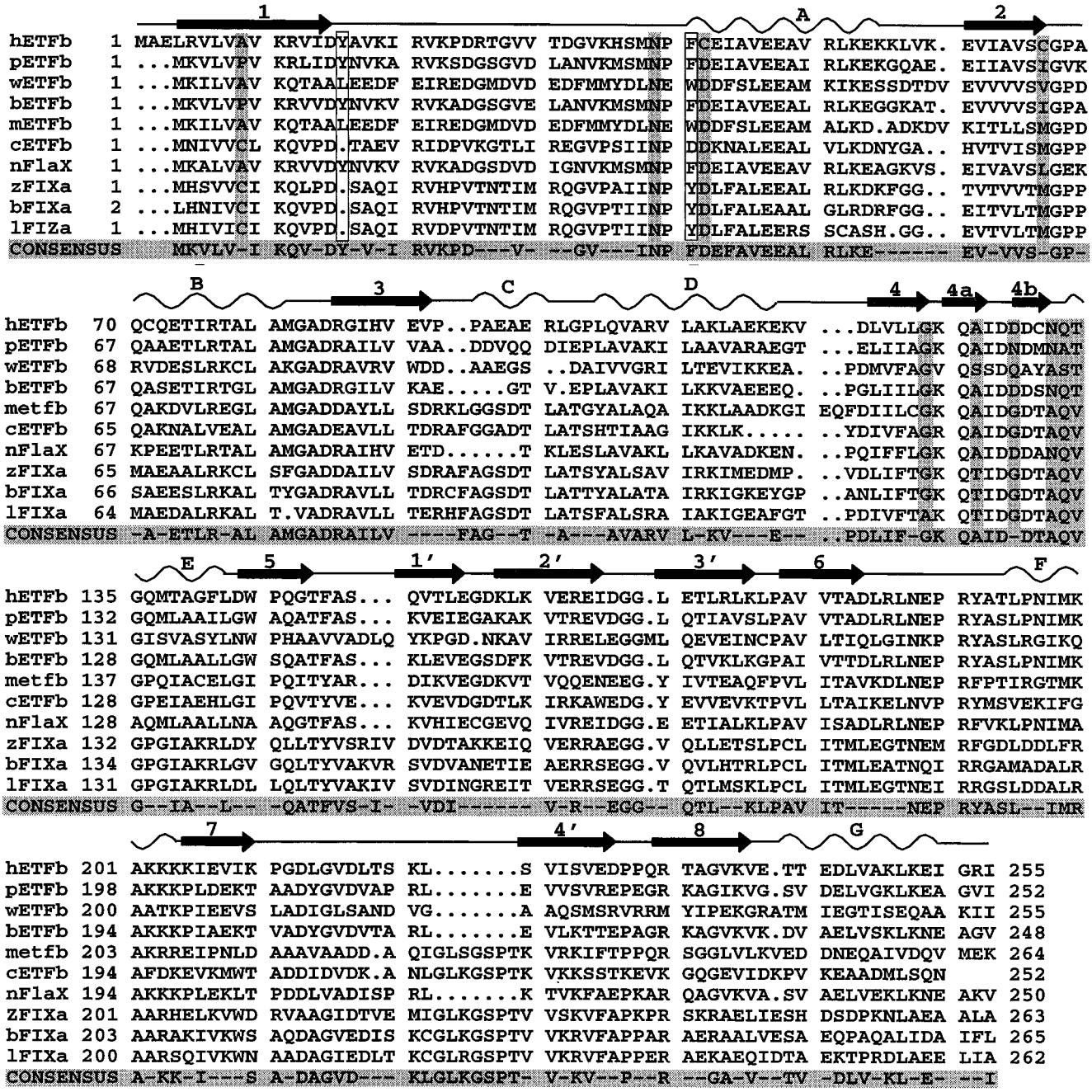

FIGURE 3: Structure-based amino acid sequence alignment for members belonging to the ETF family of proteins. The alignment was initially generated utilizing the BESTFIT algorithm (Genetics Computer Group program, University of Wisconsin—Madison). The output was modified such that gaps and insertions were placed in loop regions. The secondary structure of the ETF protein is shown above the sequence. The arrows designate β-strands, and the wavy lines represent α-helices. The secondary structure labeling scheme is the same as that developed for the human ETF protein (*10*). The consensus sequence (shaded below the alignments) indicates residues that are identical in at least five of the nine sequences shown. (A, left page) Sequence alignment of the α-subunit of ETF and the putative FixB protein. Sixteen known sequences were used to generate the alignment, and only nine representative sequences are shown here, due to limited space. Residues within the sequence that are shaded indicate those located near the isoalloxazine portion of the FAD cofactor. Boxed residues indicate those involved in binding the remainder of the FAD cofactor. Proteins displayed in the sequence alignment are as follows (Swiss-Prot ID numbers are shown in parentheses): hETFa, human ETF (P13804); pETFa, *P. denitrificans* ETF (P38974); wETFa, *Methylophilus methylotrophus* W3A1 ETF (P53571); bETFa, *Bradyrhizobium japonicum* ETF (P53573); mETFa, *Megasphaera elsdenii* ETF (gene bank ID AF072475); cETFa, *Clostridium acetobutylicum* ETF (P52039); zFIXb, *Azotobacter vinelandii* FixB protein (P53574); bFIXb, *B. japonicum* FixB protein (P10449); and cFIXb, *C. acetobutylicum* FixB protein (P53578). Other proteins used to initially generate the alignment were the following: *Bacillus subtilis* ETF (P94551); *Caenorhabditis elegans* ETF (Q93615); *Clostridium thermosaccharolyticum* ETF (P71153); *Schizosaccharomyces pombe* ETF (P78790); *Saccharomyces cerevisiae* ETF (Q12480); *Azorhizobium caulinodans* FixB (P26483); and *Rhizobium meliloti* FixB (P09819). (B, right page) Sequence alignment of the β-subunit of ETF and the putative FixA protein. Fifteen known sequences were used to generate the alignment, and 10 representative sequences are shown due to limited space. Shaded residues indicate those that define the AMP binding site in human and *P. denitrificans* ETF. Boxed residues indicate those from the β-subunit that interact with the isoalloxazine portion of the FAD cofactor. Proteins displayed in the sequence alignment are as follows (Swiss-Prot ID numbers are shown in parentheses): hETFb, human ETF (P38117); pETFb, *P. denitrificans* ETF (P38975); wETFb, *M. methylotrophus* W3A1 ETF (P53570); bETFb, *B. japonicum* ETF (P53575); mETFb, *M. elsdenii* ETF (gene bank ID AF072475); cETFb, *C. acetobutylicum* ETF (P52040); nFlaX, *Neisseria meningitidis* FlaX gene product (U40862); zFixA, *A. vinelandii* FixA protein (P53576); bFixA, *B. japonicum* FixA protein (P53577); and lFixA, *Rhizobium leguminosarum* FixA protein (Q05559). Other proteins used to initially generate the alignment were the following: *B. subtilis* ETF (P94550); *C. thermosaccharolyticum* ETF (P97089); *S. cerevisiae* ETF (P42940); *A. caulinodans* FixB (P26482); and *R. meliloti* FixB (P09818).

FIGURE 4: Stereo ribbon diagram of the ETF structure showing electrostatic differences between the human and *P. denitrificans* enzymes. The locations of residues that exhibit a change in charge (either negative−positive, negative−neutral, positive−negative, positive−neutral, neutral−negative, or neutral−positive) are mapped onto the ribbon diagram and displayed in black. The majority of changes are located within domain I, while the "top" surface of the molecule, which was previously hypothesized to interact with MCAD, has the least changes. The portion of the β-subunit that was substituted for to make the chimeric ETF protein is indicated as a dark gray ribbon. FAD and AMP are shown in black ball-and-stick models.

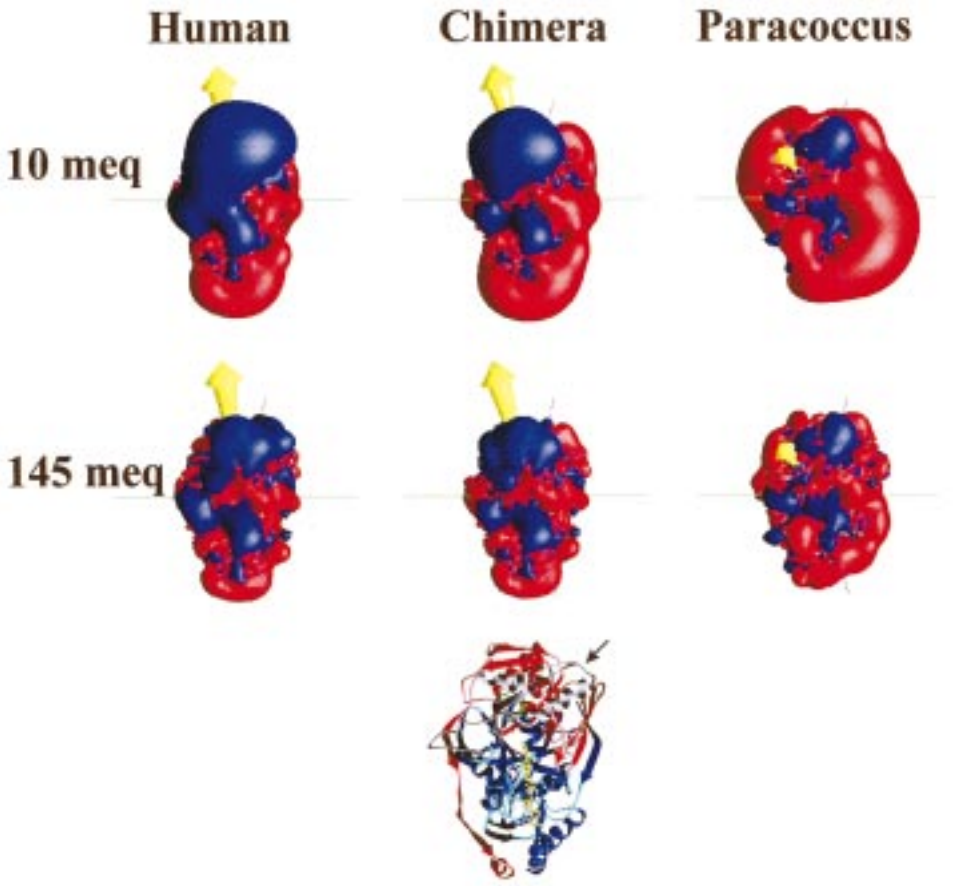

FIGURE 5: Electrostatic potentials of the ETF proteins. The surface potentials were calculated at varying ionic strengths, all at pH 8.0. Red indicates negative charge, while blue is indicative of positive charge. Yellow arrows indicate the magnitude and direction of the dipole moment calculated for the proteins. The ionic strengths are as follows: top row, 10 mequiv; middle row, 145 mequiv. A ribbon diagram with coloring as in Figure 1 is shown in the bottom row to clarify the orientation. The portion of the β-subunit that was substituted for to make the chimeric ETF is shown in gray ribbon as in Figure 4, and the arrow indicates the location of the charge differences in chimeric ETF from human ETF. The surfaces were calculated for human ETF (first column), chimeric ETF (middle column), and *P. denitrificans* ETF (last column).

ETF-QO have been shown to be at least partially electrostatic in nature (*35*). *P. denitrificans* ETF has been reported to be incapable of reducing mammalian ETF-QO, presumably due to differences in surface complementarity, since the potentials for the human and bacterial ETFs are very similar. Furthermore, a chimeric human−*Paracoccus* ETF has been described in which the amino-terminal third of the β-subunit contains residues of the bacterial ETF; the remaining β-subunit and the entire α-subunit contain the human sequence (*19*; see Figures 4 and 5). The value of k_{cat}/K_m of ETF-QO is 150-fold less with the chimeric ETF than with human ETF, although the circular dichroism spectra indicate

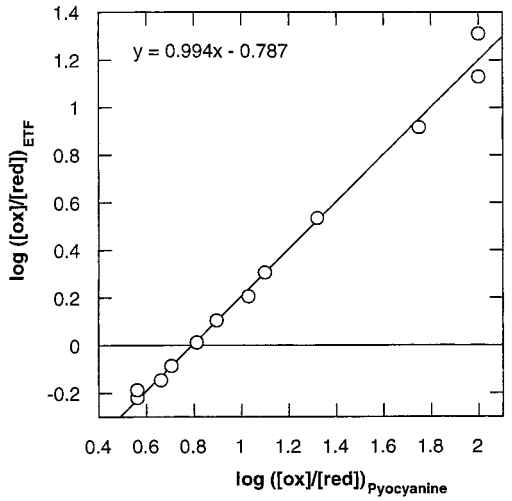

FIGURE 6: Determination of the oxidation/reduction potential of *P. denitrificans* ETF. The potential was determined by the method of Massey (*31*), using 20 μM ETF, 20 μM pyocyanine, 0.25 mM xanthine, 30 nM xanthine oxidase, and 1.5 μM benzyl viologen in 10 mM potassium phosphate buffer, pH 7.0, containing 5% glycerol. The reaction was run at 10 °C.

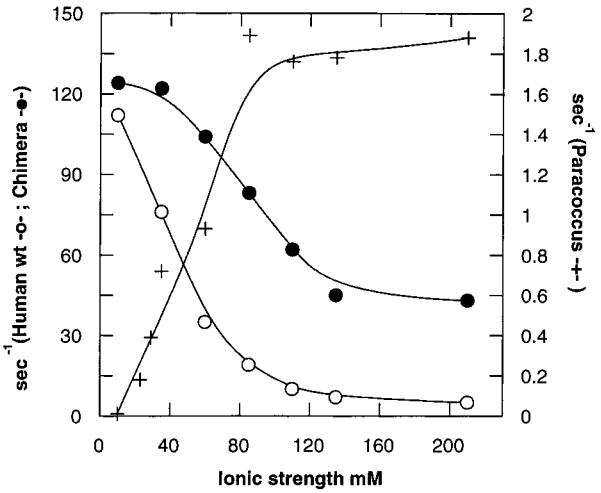

FIGURE 7: Reduction of human ETF, *P. denitrificans* ETF, and human−*P. denitrificans* chimeric ETF (*19*) by medium-chain acyl-CoA dehydrogenase. The rate of reduction of the three ETFs as a function of ionic strength was determined fluorometrically under anaerobic conditions. The concentration of all three ETFs was held constant at 1 μM, and the ionic strength was varied by addition of NaCl to the buffer. Reactions were initiated by the addition of medium-chain acyl-CoA dehydrogenase; the symbols indicate human ETF (○), *P. denitrificans* ETF (+), and the chimeric ETF (●).

the flavin environments are essentially identical in the two proteins. Inspecting the electrostatic surfaces, it seems clear that the only real charge difference between the human and chimeric ETFs is in the top right-hand portion of the ETF molecule, as shown in Figure 5. This region is located within the "back" of the β-subunit (domain III) as shown in Figure 1. Careful analysis of residues that may be responsible for this difference reveals that Lys56 and Lys59 of the human enzyme are replaced by Gly and Glu, respectively, in the *P. denitrificans* structure (see the ribbon diagram in Figure 5). These residues are located on the surface and are in a variable region of the ETF sequences. Therefore, it seems that the loop between helix A and strand 2 of the β-subunit participates at least in part with binding to ETF-QO.

Effects of Electrostatic Protein Surface Potentials on Kinetic Properties of ETFs. The oxidation/reduction potentials for several ETFs have been determined. Values range from +0.219 and −0.220 V for the transfers of the first and second electrons to the ETF of *Methylophilus methylotrophus*, a methylotroph closely related to W3A1, to near zero volts for the couples of pig and human ETFs (*11, 12*). For *P. denitrificans* ETF, the two-electron oxidation/reduction potential was estimated to be -0.021 ± 0.003 V (Figure 6). The slope of the line in Figure 6 is 0.96, which is close to the expected value of 1.0 for a two-electron system with a two-electron indicator, and Nernst plots of the data yielded a slope of 0.030 ± 0.003. This small difference in potential between human and *Paracoccus* ETFs is consistent with the close similarity of the flavin surroundings.

Inert electrolytes modify the electrical field of the proteins and therefore alter the protein−protein interactions. The apparent second-order rate constants, estimated from k_{cat}/K_m for the reaction of porcine ETF with its homologous electron donor, MCAD, and its electon acceptor, ETF-QO, are highly dependent on ionic strength (*34, 35*). The effect of ionic strength on k_{cat}/K_m is almost entirely the result of a large increase in K_m of MCAD and ETF-QO for ETF. The effect of ionic strength on k_{cat} is relatively small. Earlier experiments of Husain and Steenkamp (*3*) demonstrated that *P. denitrificans* ETF could serve as an electron acceptor for mammalian dehydrogenases but did not exhibit saturation behavior with all of these dehydrogenases. Figure 7 compares the ionic strength dependence of the reaction of MCAD with human ETF, *P. denitrificans* ETF, and a human−*Paracoccus* chimeric ETF (*19*); all reactions were conducted at 1 μM ETF at pH 8.0, the pH optimum for the dehydrogenase. It shows that the rates of reduction with human and chimeric ETFs decrease as ionic strength increases, while the rate with *P. denitrificans* ETF decreases. The effect of ionic strength on the reaction with the chimeric ETF is not as profound as on the two wild-type ETFs. Since the net charge difference between the chimeric sequence and the human sequence is −3 (Figure 4), the experiment gives some insight into the contribution of negatively charged residues in this region of the β-subunit to the protein−protein interaction. Because the docking site for MCAD (*10*) is almost identical in all three proteins, the results suggest that the effect of ionic strength is exerted on long-range forces between ETFs and MCAD. These long-range forces reflect the predominantly negative surface potential of *Paracoccus* ETF and the overall neutral surface potential of human ETF. The results are similar to the effects of ionic strength on the reduction of the positively charged cytochrome *c* and the negatively charged plastocyanin by the cytochrome *bf* complex. However, in the reaction of plastocyanin and the cytochrome *bf* complex, the results are apparently due to local charges on the redox proteins in the electron transfer complex and therefore short-range forces (*47*).

The original description of *P. denitrificans* ETF indicated that the bacterial ETF did not reduce mammalian (pig) ETF-QO when assayed as a ubiquinone reductase (*3*). The ionic strength dependence of the reactions of *P. denitrificans* ETF with pig MCAD makes the early experiments difficult to interpret because the reduced ETF substrate of pig ETF-QO was generated by an acyl-CoA dehydrogenase and the appropriate substrate. In the present work, direct assay of *P.*

denitrificans and human ETF semiquinones as substrates of pig ETF-QO in the disproportionation reaction catalyzed by ETF-QO has shown that the bacterial enzyme is a substrate of pig ETF-QO and that the ionic strength dependence of the disproportionation of the two ETF substrates is very similar to that shown in Figure 7 for the reaction of MCAD with the two ETF substrates (data not shown). Whether the ionic strength dependency in the reaction of ETF and ETF-QO is due to long-range forces or due to local charges cannot be determined at present.

SUMMARY

In this paper we have determined the structures of the *P. denitrificans* ETF protein. Comparing this structure to the structure of the human ETF has permitted additional insight into the nature of electron transfer between ETF and its redox partners. In addition, on the basis of sequence alignments throughout the ETF family and the conservation of three-dimensional structure among two members with very different surface charge, it is likely that the immediate flavin environment is responsible for preservation of flavin chemistry such as anion semiquinone stabilization. However, it is a combination of contact residues and more remote charged residues that modulate redox potentials and electron donor/acceptor specificity.

By analysis of the surface charge complementarity between both human and *P. denitrificans* ETF and MCAD, it is possible to support previous docking studies looking for residues involved in contact between ETF and MCAD. As in the case of human ETF, the flavin rings of ETF and MCAD are separated by approximately 19 Å. Residues that may participate in electron transfer from MCAD to *P. denitrificans* ETF include W166, E212, and R210 of MCAD and αD231 and αR227 of the ETF protein. According to this model, the electrons flow from the *si* face of the MCAD FAD to the *re* face of the ETF flavin. Furthermore, from these studies it is possible to identify a portion of the docking site between ETF and its electron acceptor, ETF-QO. While the ETF-QO docking site may overlap with that of MCAD, a portion of the docking site is located in the N-terminal portion of the β-subunit (K56 and K59), in the loop between helix A and strand 2. Further studies are presently underway to understand the nature of docking between ETF and ETF-QO.

REFERENCES

1. Weidenhaupt, M., Rossi, P., Beck, C., Fischer, H.-M., and Hennecke, H. (1996) *Arch. Microbiol. 165*, 169−178.
2. Crane, F. L., and Beinert, H. (1956) *J. Biol. Chem. 218*, 717−731.
3. Husain, M., and Steenkamp, D. J. (1985) *J. Bacteriol. 163*, 709−715.
4. Bedzyk, L. A., Escudero, K. W., Gill, R. E., Griffin, K. J., and Frerman, F. E. (1993) *J. Biol. Chem. 268*, 20211−20217.
5. Chen, D., and Swenson, R. P. (1994) *J. Biol. Chem. 269*, 32120−32130.
6. Eichler, K., Buchet, A., Bourgis, F., Kleber, H. P., and Mandrand-Berthelot, M. A. (1995) *J. Basic Microbiol. 35*, 217−227.
7. Tsai, M. H., and Saier, M. H., Jr. (1995) *Res. Microbiol. 146*, 397−404.
8. Earl, C. D., Ronson, C. W., and Ausubel, F. M. (1987) *J. Bacteriol. 169*, 1127−1136.
9. Preisig, O., Anthamatten, D., and Hennecke, H. (1993) *Proc. Natl. Acad. Sci. U.S.A. 90*, 3309−3313.
10. Roberts, D. L., Frerman, F. E., and Kim, J. J.-P. (1996) *Proc. Natl. Acad. Sci. U.S.A. 93*, 14355−14360.
11. Salazar, D., Zhang, L., deGala, G. D., and Frerman, F. E. (1997) *J. Biol. Chem. 272*, 26425−26433.
12. Husain, M., Stankovich, M. T., and Fox, B. G. (1984) *Biochem. J. 219*, 1043−1047.
13. Byron, C. M., Stankovich, M. T., Husain, M., and Davidson, V. (1989) *Biochemistry 28*, 8582−8587.
14. Salazar, D., Zhang, L., and Frerman, F. E. (1997) in *Flavins and Flavoproteins* (Stevenson, K. J., Massey, V., and Williams, C. H., Jr., Eds.) pp 93−96, University of Calgary Press, Alberta, Canada.
15. Griffin, K. J., Dwyer, T. M., Manning, M. C., Meyer, J. D., Carpenter, J. F., and Frerman, F. E. (1997) *Biochemistry 36*, 4194−4202.
16. Sato, K., Nishina, Y., and Shiga, K. (1993) *J. Biochem. 114*, 215−222.
17. DuPlessis, E. R., Rohlfs, R. J., Hille, R., and Thorpe, C. (1994) *Biochem. Mol. Biol. Int. 32*, 195−199.
18. Swenson, R. P., and Chen, D. (1997) in *Flavins and Flavoproteins* (Stevenson, K. J., Massey, V., and Williams, C. H., Jr., Eds.) pp 515−518, University of Calgary Press, Alberta, Canada.
19. Herrick, K. R., Salazar, D., Goodman, S. I., Finocchiaro, G., Bedzyk, L. A., and Frerman, F. E. (1994) *J. Biol. Chem. 269*, 32239−32245.
20. Zhou, Z., and Swenson, R. P. (1995) *Biochemistry 34*, 3183−3192.
21. Chang, F. C., and Swenson, R. P. (1997) *Biochemistry 36*, 9013−9021.
22. Ludwig, M. L., Pattridge, K. A., Metzger, A. L., Dixon, M. M., Eren, M., Feng, Y., and Swenson, R. P. (1997) *Biochemistry 36*, 1259−1280.
23. Roberts, D. L., Herrick, K. R., Frerman, F. E., and Kim, J. J.-P. (1995) *Protein Sci. 4*, 1654−1657.
24. McPherson, A. (1990) *Eur. J. Biochem. 189*, 1−23.
25. Matthews, B. W. (1968) *J. Mol. Biol. 33*, 491−497.
26. Otwinowski, Z., and Minor, W. (1996) in *Methods of Enzymology* (Carter, C. W., Jr., and Sweet, R. M., Eds.) Vol. 276, Academic Press, New York.
27. Rossman, M. G., and Blow, D. M. (1962) *Acta Crystallogr. 15*, 24−31.
28. Brünger, A. (1992) *X-PLOR, Version 3.1*, Howard Hughes Medical Institute and Department of Biophysics and Biochemistry, Yale University, New Haven, CT.
29. Cambillau, C., Roussel, A., Inisan, A. G., and Knoops-Mouthuy, E. (1996) *TURBO−FRODO Manual (Version 5.5)*, CNRS/Universite Aix-Marseille, Marseille, France.
30. Nichols, A. (1992) *GRASP: Graphical Representation and Analysis of Surface Properties*, Columbia University, New York.
31. Massey, V. (1991) in *Flavins and Flavoproteins* (Curti, B., Ronchi, S., and Zanetti, G., Eds.) pp 59−66, Walter de Gruyter, Berlin.
32. McIlwain, H. (1937) *J. Chem. Soc. 2*, 1704−1711.
33. Minnaert, K. (1965) *Biochim. Biophys. Acta 110*, 42−56.
34. Beckmann, J. D., and Frerman, F. E. (1983) *J. Biol. Chem. 258*, 7563−7569.
35. Beckmann, J. D., and Frerman, F. E. (1985) *Biochemistry 24*, 3922−3925.
36. Carson, M. (1996) *RIBBONS, Version 2.0*, University of Alabama, Birmingham, AL.
37. Whitfield, C. D., and Mayhew, S. G. (1974) *J. Biol. Chem. 249*, 2801−2810.
38. O'Neill, H., Mayhew, S. G., and Butler, G. (1998) *J. Biol. Chem. 273*, 21015−21024.
39. Sharkey, C. T., Walsh, M. A., Mayhew, S. G., and Higgins, T. M. (1997) *Acta Crystallogr., Sect. D 53*, 461−463.
40. Gorelick, R. J., and Thorpe, C. (1986) *Biochemistry 25*, 7092−7098.
41. Moore, S. A., James, M. N., O'Kane, D. J., and Lee, J. (1993) *EMBO J. 12*, 1767−1774.

42. Lu, G., Lindqvist, Y., Schneider, G., Dwivedi, U., and Campbell, W. (1995) *J. Mol. Biol. 248*, 931−948.
43. Muller, Y. A., and Schulz, G. E. (1993) *Science 259*, 965−967.
44. Müller, F. (1992) in *Chemistry and Biochemistry of Flavoenzymes* (Müller, F., Ed.) Vol. III, pp 557−595, CRC Press, Boca Raton, FL.
45. Griffin, K. J., deGala, G. D., Eisenreich, W., Müller, F., and Frerman, F. E. (1998) *Eur. J. Biochem. 255*, 125−132.
46. Gatti, D. L., Palfey, B. A., Lah, M. S., Entsch, B., Massey, V., Ballou, D. P., and Ludwig, M. L., (1994) *Science 266*, 110−114.
47. Wagner, M. J., Packer, J. C., Howe, C. J., and Bendall, D. S. (1995) *Biochim. Biophys. Acta 1276*, 246−252.

BI9820917